Semi-continuous strategy for the modelling of damage mechanisms in unidirectional composites under low velocity impacts

Bassam Mahmoud, Marcos Torrecilla Colungo, Pablo Navarro, Steven Marguet, Issam Tawk, Jean-François Ferrero

Semi-Continuous strategy for the modelling of damage mechanisms in unidirectional composites under low velocity impacts

Mahmoud Bassam[a,b], Colungo Torrecilla Marcos[a], Navarro Pablo[a], Marguet Steven[a], Tawk Issam[b], Ferrero Jean-Francois[a]

[a] *Université de Toulouse, Institut Clément Ader, UMR CNRS 5312, INSA/UPS/ISAE/Mines Albi, 3 rue Caroline Aigle, 31400 Toulouse, France*
[b] *University of Balamand, Deir El-Balamand, El-Koura, Lebanon*

Abstract

This article deals with the development of a finite element model for the prediction of low velocity impact damage within unidirectional composite laminates. This model is based on analysis of the impact damage observed experimentally. The modelling scale is that of the bundle of fibers of the unidirectional ply. These bundles are represented with 1D rod elements. The matrix is modeled with 2D damageable shell elements. The laminate is the built using cohesive elements. The strategy is validated by a comparison with low velocity drop weight impact tests. Several experimental parameters are varied : the materials (T700/M21 and HTA7/913), the thickness ($1.44mm$ and $2.4mm$), the stacking sequence and the impact velocity ($2m.s^{-1}$ and $3m.s^{-1}$). The calculated load-displacement curves and the damage extent correlate well with experimental results.

Keywords:

A. Carbon fibre, B. Impact behaviour, C. Finite element analysis (FEA), C. Damage mechanics

1. Introduction

This article deals with the modelling of impacts on composite laminates made with unidirectional layers. The work focuses on the development of a specific Finite Element model able to predict damage mechanisms and chronology during impact.

Composite materials are widely used in many applications, especially where high strength and stiffness to weight ratio is concerned. This material characteristics is interesting for a wide range of industries, particularly in the transport industry such as aircrafts, helicopters, boats or cars. However, when submitted to low energy impacts, composite laminates exhibit a relatively brittle behaviour with extensive matrix cracking, delamination or fibers breakages [1, 2, 3]. This damage can lead to a loss of stiffness and eventually a loss of load carrying capability when fibers break. Usually, these damages are defined as intralaminar damages (inside the ply: matrix cracking, fiber and matrix debonding, fiber breakages), and as interlaminar damages (between plies with two different orientations: delamination). Considering the time and cost of physical testing, the prediction of composite impact damage is still a challenge.

Several authors have performed detailed reviews on impact modelling approches [4, 5]. They can be divided in three different areas. First, the failure criteria approaches [6, 7, 8], based on an equivalent stress or strain, are classically used to describe the failure of multidirectional laminates subjected to multi axial loading. Nevertheless, these approaches cannot characterize the damage mechanisms resulting from an impact loading. Then, the fracture

mechanics approaches [9, 10, 11, 12] provide interesting results but causes difficulties like a sensitivity to the mesh size. Finally, the damage mechanics approaches [13, 14, 15, 16, 17, 18, 19, 20, 21, 22, 23, 24] successfully predict matrix cracking and delamination responsible for stiffness degradation. The simulation of the delamination is usually made using interface elements [25, 26, 27, 28, 29]. Wisnom [30] and Abrate [31] have provided detailed reviews on the use of cohesive zone interface elements to model matrix failures in polymer composites. Cohesive zone elements capture correctly the form and propagation of delamination at the interface of adjacent plies through the definition of adapted damage initiation and evolution laws [32, 33]. This strategy was used successfully for the modelling of low and high velocity impact damages on preloaded samples [34, 35]. Interface elements can also be used to model transverse matrix cracks when positioned vertically [36, 37]. It allows a precise representation of intralaminar and interlaminar impact damages. Nevertheless, the use of vertical interfaces often leads to a complex mesh that cannot be implemented easily. More, the results provided by this modelling approach highly depends on the position and the number of the out of plane cohesive elements.

Thus, a new modelling approach, called semi-continuous strategy, and described in [38, 39, 40] has been developed. The modelling scale is that of the bundles of fibers. It is chosen to represent the impact damage observed experimentally, so that the use of vertical interfaces is avoided. The fiber and matrix mechanical behaviors are separated. The fibers are modelled with rod elements and a specific damageable shell element is used to stabilize the rod elements. This strategy allows a precise representation of the damage

chronology within the material.

In this paper, an extension of that semi-continuous approach, initially developed for woven composites, is described and implemented into the finite element code Radioss to predict damage mechanisms in unidirectional composites under low velocity impacts. The numerical development presented here are part of an overall work that aims, eventually, to study and model impacts on hybrid woven/unidirectional laminates. As a consequence, the proposed model has been set up in order to be fully compatible with the modelling approach for woven composites described in [38, 39, 40].

In the first part, the modelling strategy is presented. The damage law used for the developed shell elements and the failure behaviour of the rods are described. Then, the drop weight impact tests used to validate the modelling strategy, and performed on T700/M21 and HTA7/913 composites, are described. Finally the results from calculation are presented and compared to experimental results. A good correlation is found. This demonstrate the ability of the proposed approach to predict the type and the extent of impact induced damage.

2. Model description

In this part, a detailed description of the proposed Uni-Directional ply modelling is provided.

2.1. Principle

The modelling principle is based on a Semi-Continuous strategy, as described in [38]. It relies on experimental observations of the failure of Uni-Directional plies under impacts. A fracture surface of a Uni-Directional thin

laminate after impact is given in Figure 1. The damage scenario can be described in three main steps. First, the resin is damaged. Longitudinal cracks propagating between the fibers are observed. The groups of fibers between these cracks, that constitutes bundles of fibers, are not stabilized anymore by the resin. They behave independently, carrying mainly tensile and compressive loads. Finally, these bundles of fibers fail in tension when the ultimate strain of the material is reached.

The modelling has to represent this damage scenario, and particularly unstabilized bundles. Thus, the proposed modelling strategy relies on a representation of the bundles of fibers with 1D rod elements, stabilized with a specific 2D shell element that can be damaged. The modelling scale is that of the size of the bundles of fibers : the mesh size corresponds to the distance between two longitudinal cracks. A description of the modelling is given in Figure 2 .

2.2. Rod elements description

A brittle linear elastic law is chosen to represent the behavior of the bundle of fibers. The elastic modulus E_f is that of the fiber material. It is given by the manufacturer. The section area of the rods is calculated from the fiber volume fraction V_f of the considered ply.

The bundle rupture is assumed to be brittle in tension. Therefore, a classic maximum tensile strain criterion is used for the rupture of the rods. The maximal strain ε_{max} is identified from static and dynamic tensile tests. In order to avoid numerical instabilities, when the maximum strain criterion is reached, the normal force F_N in the rod is smoothly decreased by the use

of a characteristic time τ as follow:

$$F_N(t) = F_N^* \left(1 - \exp \frac{t^* - t}{\tau}\right) \tag{1}$$

where t^* is the exact time at which the criterion is reached and F_N^* the force stored at time t^*. This law is plotted in Figure 3. The failure in compression is not considered.

2.3. Shell element description

The role of shell elements is to stabilize the bundles of fibers. The behavior of these elements is peculiar to the semi-continuous modelling strategy, so that their formulation was specifically developped for the proposed approach. The elements behave like the homogenized ply for the bending loading, shearing loading and membrane transverse loading (in the direction perpendicular to the fibers). In that case, the elastic properties are identified from static and dynamic tensile tests. For the membrane loading in the direction of the fibers, the elements behave like the resin.

The construction of this element is based on orthotropic shell theory and on Belytschko's formulation. Four integration points are used.

This element is damageable. The damage formulation introduced is based on damage mechanics. The initiation and propagation laws relies on the developments of Ladeveze and Allix, described in [13, 14]. Two damage variables, d_L and d_T are used. These variables represent the microcrack apparition and propagation in the longitudinal and transverse directions (L and T), as explained in Figure 4 . d_L and d_T vary between 0 (when the shell is not damaged) and 1 (when the shell is totally damaged). In order to model the loss of stiffness, these two damage variables degrade membrane,

bending and out of plane moduli. The Poisson's ratio are also damaged. As a consequence, the membrane, bending and out of plane shear stress-strain relationships are defined by :

$$\left\{ \begin{array}{c} \sigma^m_{LL} \\ \sigma^m_{TT} \end{array} \right\} = \frac{1}{1-\nu_{LT}\nu_{TL}} \left[\begin{array}{cc} E^m_L & \nu_{LT}E^m_L \\ \nu_{TL}E^m_T & E^m_T \end{array} \right] \left\{ \begin{array}{c} \varepsilon^m_{LL} \\ \varepsilon^m_{TT} \end{array} \right\} \tag{2}$$

$$\left\{ \begin{array}{c} \sigma^b_{LL} \\ \sigma^b_{TT} \end{array} \right\} = \frac{1}{1-\nu_{LT}\nu_{TL}} \left[\begin{array}{cc} E^b_L & \nu_{LT}E^b_L \\ \nu_{TL}E^b_T & E^b_T \end{array} \right] \left\{ \begin{array}{c} \varepsilon^b_{LL} \\ \varepsilon^b_{TT} \end{array} \right\} \tag{3}$$

$$\left\{ \begin{array}{c} \sigma_{LZ} \\ \sigma_{TZ} \end{array} \right\} = \left[\begin{array}{cc} G_{LZ} & 0 \\ 0 & G_{TZ} \end{array} \right] \left\{ \begin{array}{c} 2\varepsilon_{LZ} \\ 2\varepsilon_{TZ} \end{array} \right\} \tag{4}$$

$$\text{with} \left\{ \begin{array}{l} E^m_L = (1-d_L)E^{m0}_L \\ E^m_T = (1-d_T)E^{m0}_T \\ E^b_L = (1-d_L)E^{b0}_L \\ E^b_T = (1-d_T)E^{b0}_T \\ \nu_{LT} = (1-d_L)\nu^0_{LT} \\ \nu_{TL} = (1-d_T)\nu^0_{TL} \\ G_{LZ} = (1-d_L)G^0_{LZ} \\ G_{TZ} = (1-d_T)G^0_{TZ} \end{array} \right. \tag{5}$$

Where σ^m_{ii} and σ^b_{ii} are respectively the membrane and bending stresses; ε^m_{ii} and ε^b_{ii} are the membrane and bending strain; σ_{iZ} and ε_{iZ} are the out of plane stress and strain; E^{m0}_L and E^{m0}_T are the membrane longitudinal and transverse undamaged elastic moduli; E^{b0}_L and E^{b0}_T are the bending longitudinal and transverse undamaged elastic moduli; G^0_{LZ} and G^0_{TZ} are the undamaged out of plane shear moduli; ν^0_{LT} and ν^0_{TL} are the undamaged Poisson ratios.

The damage variables are function of the energy release rates Y_L and Y_T, calculated from the elastic energy W_e :

$$Y_i = \frac{\partial W_e}{\partial d_i} \qquad \text{with} \qquad i \in (L,T) \tag{6}$$

The damage evolution is given by :

$$\begin{cases} d_i = \dfrac{\langle \sqrt{Y_i} - \sqrt{Y_{Oi}} \rangle_+}{\sqrt{Y_{Ci}}} & \text{if } d_i < 1 \\ d_i = 1 & \text{otherwise} \end{cases} \qquad i \in (L,T) \tag{7}$$

where Y_{Oi} ($i \in (L,T)$) controls the initiation of the degradation and Y_{Ci} ($i \in (L,T)$) controls the final rupture. The damage parameters are identified with a reverse engineering method from static and dynamic indentation tests.

Finally, the behavior of unidirectional composites in plane shear is implemented. It presents a non linear behavior, called pseudo-plasticity, characterized by the apparition of an inelastic shearing strain. To account for pseudo-plasticity in the calculation, the total in-plane shear strain ε^t_{LT}, calculated from the displacement of the nodes, is split into an elastic strain ε^e_{LT} and an inelastic strain ε^p_{LT}.

$$\varepsilon^t_{LT} = \varepsilon^e_{LT} + \varepsilon^p_{LT} \tag{8}$$

The in-plane shear stress is calculated from the elastic in plane shear. Thus the proportion between elastic strain and plastic strain has to be estimated. The calculation of these strains is carried out in two principal steps. Firstly, in an elastic prediction step, the strain increment is assumed to be purely elastic. Secondly, an elastic field, given equ 9, is used to verify the nature of the stress computed under the elastic prediction.

$$f = |\sigma_{LT}| - K_{plas}(\varepsilon^p_{LT})^\beta - \sigma_0 \tag{9}$$

where σ_{LT} is the in plane shear stress, σ_0 the plastic strength, and (K_{plas}, β) are material parameters defining the hardening law. These material parameters are identified from static and dynamic tensile tests on laminates oriented at 45° and −45° from the traction axis. If $f > 0$, a plastic correction is carried out using a Newton-Raphson iterative scheme to find the value of the plastic strain.

Besides, a third damage variable (d_{LT}) has been implemented in order to model the final in plane shear failure when the other stiffnesses are totally damaged :

$$\sigma_{LT} = 2(1 - d_{LT})G_{LT}.\varepsilon^e_{LT} \quad \text{with} \quad \begin{cases} d_{LT} = 0 \text{ if } \max(d_L, d_T) < 1 \\ d_{LT} = 1 \text{ if } \max(d_L, d_T) = 1 \end{cases} \tag{10}$$

where G_{LT} is the undamaged in plane shear elastic modulus.

2.4. Cohesive elements

The laminate is built by connecting each unidirectional ply with specific shell-to-shell interface elements. These elements, described in detail in [39], are 8-node elements with three translational and three rotational degrees of freedom per node, which allows feasible connection to shell elements. The idea is to take into account the thickness of the connected shells. Eight virtual nodes representing the physical interface are created. The assumption is made that the straight lines normal to the mid-surface of the plies remain normal, so that the virtual nodes are connected to the real nodes with rigid body elements. The reaction forces and momentum applied on the real nodes are deduced from the reaction forces applied on the virtual nodes. The principle is illustrated in figure 5. In the present work, the cohesive constitutive

law used is a bilinear traction separation law. It consists of an initial linear elastic stage until damage initiation, followed by a linear softening phase that represent progressive delamination. The evolution of damage was monitored by a damage variable (d_{int}), ranging from the values 0 to 1, so that :

$$\begin{Bmatrix} \sigma_n^{int} \\ \sigma_s^{int} \\ \sigma_t^{int} \end{Bmatrix} = (1 - d_{int})K \begin{Bmatrix} \delta_n \\ \delta_s \\ \delta_t \end{Bmatrix} \tag{11}$$

Where K is the stiffness of the interface ; σ_i^{int} and δ_i represents respectively the interface stress and the displacement discontinuities and where the subscripts n, s and t denotes respectively the mode I, II and III directions. The initiation criterion is a stress based quadratic criterion (equ 12) and the propagation follows a linear energy-based interaction law (equ 13):

$$\left(\frac{\sigma_n^{int}}{\sigma_I^0}\right)^2 + \frac{(\sigma_s^{int})^2 + (\sigma_t^{int})^2}{(\sigma_{II}^0)^2} = 1 \tag{12}$$

$$\frac{G_I}{G_{Ic}} + \frac{G_{II} + G_{III}}{G_{IIc}} = 1 \tag{13}$$

Where σ_I^0 and σ_{II}^0 are the interface strengths under modes I and II; G_I, G_{II} and G_{III} are the energy release rate in modes I, II and III; G_{Ic} and G_{IIc} are the critical energy release rates. The parameters of the cohesive law are identified from Double Cantilever Beam and End-Notched Flexure tests.

3. Validation of the modelling with low velocity impact tests

In this part, drop weight normal impact tests are performed in order to validate and evaluate the accuracy of the proposed modelling.

3.1. Drop weight impact tests description

Low velocity impact tests have been performed with a drop tower device (Figure 6). The mass of the impactor is $2\,kg$. It is hemispherical with a diameter of 16 mm. The samples are rectangular laminates with a size of $100 \times 150\,mm^2$. The specimen is simply supported on a $75 \times 125\,mm^2$ rectangular frame. The impact reaction load and the displacement of the impactor are measured during the test. The bottom of the sample is filmed with a high speed camera (Photron FastCam APX RS) at a frame rate of $20000\,fps$. Computed tomography is used after the test to observe resin cracks, fiber failure and delamination within the impacted samples. The voxel size is about $60\,\mu m$.

The purpose of these tests is to assess the modelling accuracy. Thus various test configurations have been tested. The varied parameters are the material, the laminate thickness, the stacking sequence and the impact velocity.

First, two different materials, largely used in the aeronautic industry, are tested:

- HTA7/913 Uni-Directional composite : it is made up of carbon fibers and of heat-hardening resin.
- T700/M21 Uni-Directional composite : it is made up of high strength carbon fibers and of mixed heat-hardening and thermoplastic resin.

Then, six different stacking sequences, corresponding to two laminate thicknesses are investigated:

- Four stacking sequences with a laminate thickness of $1.44\,mm$: $[0_2, 90_2, 0_2]$, $[90_2, 0_2, 90_2]$, $[0_2, 45_2, 0_2]$, $[90_2, 45_2, 90_2]$.
- Two stacking sequences with a laminate thickness of $2.4\,mm$: $[0_2, 90_2, 0_2, 90_2, 0_2]$, $[90_2, 0_2, 90_2, 0_2, 90_2]$

Finally, two impact velocities are tested : $2\,m.s^{-1}$ $(4\,J)$ and $3\,m.s^{-1}$ $(9\,J)$.

A list of the impacted configurations with the corresponding impact velocity is given in Table 1.

3.2. Modelling description

The low velocity impact tests presented above are modeled using the Semi-Continuous strategy presented in Section 2, on the explicit FEM software Radioss. The laminate is built using the specific cohesive element presented in [39]. The mesh size is $1\,mm$. It corresponds to the size of the bundles of fibers. The impactor and the rigid frame are modeled using rigid surfaces. The contact between the impactor and the laminate, between the frame and the laminate, and between the plies is accounted for. The computational time is about 20 minutes on 120 cores from HPC ressources (supercomputing centre CALMIP).

The material parameters used for the calculation are given in Table 2 and in Table 3.

4. Results and discussion

In this part, a comparison between experimental and numerical results is achieved. For the sake of clarity and conciseness, detailed results and analyzes are provided for a selection among the ten impacted configurations. The

choosen configurations represent the entirety of the investigated parameters. Furthermore, relative errors between experimental and numerical results for the maximum load (F_{max}), the maximum impactor displacement (u_{max}) and the maximal size of delamination (Ld_{max})are given for all the configurations in Table 4.

4.1. Load/Displacement curves

The numerical and experimental load/displacement curves for the configurations S1, S3, S6 and S10 are given in Figure 7.

These curve are divided in two main steps. First the load increases linearly with the impactor displacement until a maximal value. Then the impactor rebounds and the load decreases.

A good correlation is found between experimental and numerical results. More, the relative experimental/calculation errors provided in Table 4 are under 7.3 % for the maximum load and under 10.2 % for the maximal impactor displacement.

4.2. Damage within the laminate

The intralaminar and interlaminar damages calculated and measured with tomography are provided for two different thicknesses and impact velocities in Figure 8 for the configuration S3 and in Figure 9 for the configuration S6. The damages observed experimentally are well represented by the modelling. The modelling strategy is able to reproduce the typical shape of delamination and its size. The longitudinal cracks within the plies are also well represented. The relative experimental/calculation error provided in Table 4 for the maximal size of delamination is under 16.2 %.

Finally, for most of the tests, fiber failures are noticed experimentally within the second to last ply. These ruptures, represented with the failure of the rod elements in the modelling, are well represented. An example is given in Figure 10 for the configuration S8.

4.3. Analysis of the damage mechanisms

The mechanisms leading to the final damage map can be analyzed from both experimental and numerical results. An illustration is given in Figure 11.

- First, a longitudinal crack appears in the bottom ply. It is caused by the bending of the panel. The propagation of this crack is very fast (Figure 11.a).
- Several cracks, parallel to the fibers, appear in the other plies. Two main cracks per ply are noticed (Figure 11.b).
- Then, delamination initiates and propagates. This phenomenon occurs mainly in mode I (Figure 11.c). Indeed, the part of the upper ply between the two cracks pushes on the lower ply which opens the delamination crack.
- Finally, if the energy is high enough, a failure of the fibers within the second to last ply occurs. It corresponds to a slight drop in the load/time curve (Figure 11.d).

5. Conclusion

This article presents a semi-continuous approach for the modelling of low velocity impacts on unidirectional composites. The strategy is validated by

a comparison with low velocity drop weight impact tests. The materials, stacking sequences, thicknesses and impact velocities are varied. The calculated load-displacement curves and the damage extent correlate well with experimental results.

The originality of this strategy is that the plies are represented at the scale of the bundles of fibers. The intermediate damage state observed experimentally, where the resin is cracked and where the bundle of fibers behave independently, is well represented. Consequently, the damage within the ply can be modeled even though transverse cohesive elements, that leads to a complex meshing process, are not used. More, another contribution of this article is to provide a model for unidirectional composites fully compatible with the semi-continuous modelling strategies developed in previous work for woven composite. It makes now possible the study of hybrid unidirectional/woven laminates that could be used to improve the performances of composite structures under impact loading.

6. Acknowledgment

The authors acknowledge the supercomputing centre CALMIP for granting access to the HPC resources under the allocation 2015-P09105.

7. References

[1] E. Panettieri, D. Fanteria, M. Montemurro, C. Froustey, Low-velocity impact tests on carbon/epoxy composite laminates: A benchmark study, Composites Part B: Engineering 107 (2016) 9–21.

doi:10.1016/j.compositesb.2016.09.057.
URL http://www.sciencedirect.com/science/article/pii/S1359836816314937

[2] P. Shrestha, Y. Park, C.-G. Kim, Low velocity impact localization on composite wing structure using error outlier based algorithm and FBG sensors, Composites Part B: Engineering 116 (2017) 298–312. doi:10.1016/j.compositesb.2016.10.068.
URL http://www.sciencedirect.com/science/article/pii/S1359836816314901

[3] W. Xie, W. Zhang, N. Kuang, D. Li, W. Huang, Y. Gao, N. Ye, L. Guo, P. Ren, Experimental investigation of normal and oblique impacts on CFRPs by high velocity steel sphere, Composites Part B: Engineering 99 (2016) 483–493. doi:10.1016/j.compositesb.2016.06.020.
URL http://www.sciencedirect.com/science/article/pii/S1359836816309179

[4] S. Abrate, Impact on composite structures, Cambridge University Press, 1998.

[5] G. Davies, R. Olsson, Impact on composite structures, Aeronautical Journal 108 (1089) (2004) 541–563.

[6] Z. Hashin, Failure Criteria for Unidirectional Fiber Composites, Journal of Applied Mechanics 47 (2) (1980) 329. doi:10.1115/1.3153664.
URL http://AppliedMechanics.asmedigitalcollection.asme.org/article.aspx?artic

[7] F.-K. Chang, K.-Y. Chang, A Progressive Damage Model for Laminated Composites Containing Stress Concentrations, Journal of Composite Materials 21 (9) (1987) 834–855. doi:10.1177/002199838702100904.
URL http://jcm.sagepub.com/cgi/doi/10.1177/002199838702100904

[8] A. Puck, H. Schrmann, Failure analysis of FRP laminates by means of physically based phenomenological models, Composites Science and Technology 62 (12-13) (2002) 1633–1662. doi:10.1016/S0266-3538(01)00208-1.
URL http://linkinghub.elsevier.com/retrieve/pii/S0266353801002081

[9] J. Whitney, R. Nuismer, Stress Fracture Criteria for Laminated Composites Containing Stress Concentrations, Journal of Composite Materials 8 (3) (1974) 253–265. doi:10.1177/002199837400800303.
URL http://jcm.sagepub.com/cgi/doi/10.1177/002199837400800303

[10] E. Altus, A. Rotem, A 3-D fracture mechanics approach to the strength of composite materials, Engineering Fracture Mechanics 14 (3) (1981) 637–649. doi:10.1016/0013-7944(81)90050-3.
URL http://linkinghub.elsevier.com/retrieve/pii/0013794481900503

[11] H. Y. Choi, R. J. Downs, F.-K. Chang, A New Approach toward Understanding Damage Mechanisms and Mechanics of Laminated Composites Due to Low-Velocity Impact: Part IExperiments, Journal of Composite Materials 25 (8) (1991) 992–1011. doi:10.1177/002199839102500803.
URL http://jcm.sagepub.com/content/25/8/992

[12] M. de Moura, J. Gonalves, Modelling the interaction between matrix cracking and delamination in carbonepoxy laminates under low velocity impact, Composites Science and Technology 64 (7-8) (2004) 1021–1027. doi:10.1016/j.compscitech.2003.08.008.
URL http://linkinghub.elsevier.com/retrieve/pii/S0266353803003294

[13] P. Ladeveze, G. Lubineau, An enhanced mesomodel for laminates based on micromechanics, Composites Science and Technology 62 (4) (2002) 533–541. doi:10.1016/S0266-3538(01)00145-2.
URL http://linkinghub.elsevier.com/retrieve/pii/S0266353801001452

[14] O. Allix, L. Blanchard, Mesomodeling of delamination: towards industrial applications, Composites Science and Technology 66 (6) (2006) 731–744.

[15] S. Li, S. Reid, Z. Zou, Modelling damage of multiple delaminations and transverse matrix cracking in laminated composites due to low velocity lateral impact, Composites Science and Technology 66 (6) (2006) 827–836. doi:10.1016/j.compscitech.2004.12.019.
URL http://linkinghub.elsevier.com/retrieve/pii/S0266353804003537

[16] L. Iannucci, J. Ankersen, An energy based damage model for thin laminated composites, Composites Science and Technology 66 (78) (2006) 934–951. doi:10.1016/j.compscitech.2005.07.033.
URL http://www.sciencedirect.com/science/article/pii/S0266353805003088

[17] Y. Shi, T. Swait, C. Soutis, Modelling damage evolution in composite laminates subjected to low velocity impact, Composite Structures 94 (9) (2012) 2902–2913. doi:10.1016/j.compstruct.2012.03.039.
URL http://linkinghub.elsevier.com/retrieve/pii/S0263822312001547

[18] A. Riccio, A. De Luca, G. Di Felice, F. Caputo, Modelling the simulation of impact induced damage onset and evolution in composites, Composites Part B: Engineering 66 (2014) 340–347.

doi:10.1016/j.compositesb.2014.05.024.
URL http://www.sciencedirect.com/science/article/pii/S1359836814002376

[19] F. Caputo, A. De Luca, G. Lamanna, V. Lopresto, A. Riccio, Numerical investigation of onset and evolution of LVI damages in CarbonEpoxy plates, Composites Part B: Engineering 68 (2015) 385–391. doi:10.1016/j.compositesb.2014.09.009.
URL http://www.sciencedirect.com/science/article/pii/S1359836814004119

[20] D. Coutellier, P. Rozycki, Multi-layered multi-material finite element for crashworthiness studies, Composites Part A: Applied Science and Manufacturing 31 (8) (2000) 841–851. doi:10.1016/S1359-835X(00)00022-1.
URL http://www.sciencedirect.com/science/article/pii/S1359835X00000221

[21] D. Coutellier, J. C. Walrick, P. Geoffroy, Presentation of a methodology for delamination detection within laminated structures, Composites Science and Technology 66 (6) (2006) 837–845. doi:10.1016/j.compscitech.2004.12.037.
URL http://www.sciencedirect.com/science/article/pii/S0266353804003525

[22] F. Caputo, A. De Luca, R. Sepe, Numerical study of the structural behaviour of impacted composite laminates subjected to compression load, Composites Part B: Engineering 79 (2015) 456–465. doi:10.1016/j.compositesb.2015.05.007.
URL http://linkinghub.elsevier.com/retrieve/pii/S1359836815003017

[23] K. Zouggar, F. B. Boukhoulda, B. Haddag, M. Nouari, Numerical and experimental investigations of S-Glass/Polyester composite laminate

plate under low energy impact, Composites Part B: Engineering 89 (2016) 169–186. doi:10.1016/j.compositesb.2015.11.021.
URL http://www.sciencedirect.com/science/article/pii/S1359836815007003

[24] A. K. Bandaru, S. Ahmad, Modeling of progressive damage for composites under ballistic impact, Composites Part B: Engineering 93 (2016) 75–87. doi:10.1016/j.compositesb.2016.02.053.
URL http://www.sciencedirect.com/science/article/pii/S1359836816001724

[25] R. Borg, L. Nilsson, K. Simonsson, Simulation of low velocity impact on fiber laminates using a cohesive zone based delamination model, Composites Science and Technology 64 (2) (2004) 279–288. doi:10.1016/S0266-3538(03)00256-2.
URL http://linkinghub.elsevier.com/retrieve/pii/S0266353803002562

[26] P. P. Camanho, C. G. Davila, M. F. De Moura, Numerical Simulation of Mixed-Mode Progressive Delamination in Composite Materials, Journal of Composite Materials 37 (16) (2003) 1415–1438. doi:10.1177/0021998303034505.
URL http://jcm.sagepub.com/cgi/doi/10.1177/0021998303034505

[27] L. Iannucci, M. Willows, An energy based damage mechanics approach to modelling impact onto woven composite materials: Part II. Experimental and numerical results, Composites Part A: Applied Science and Manufacturing 38 (2) (2007) 540–554. doi:10.1016/j.compositesa.2006.02.023.
URL http://www.sciencedirect.com/science/article/pii/S1359835X06000984

[28] S. Boria, J. Obradovic, G. Belingardi, Experimental and numerical investigations of the impact behaviour of composite frontal crash structures, Composites Part B: Engineering 79 (2015) 20–27. doi:10.1016/j.compositesb.2015.04.016.
URL http://www.sciencedirect.com/science/article/pii/S1359836815002541

[29] K. T. Tan, N. Watanabe, Y. Iwahori, Finite element model for compression after impact behaviour of stitched composites, Composites Part B: Engineering 79 (2015) 53–60. doi:10.1016/j.compositesb.2015.04.022.
URL http://www.sciencedirect.com/science/article/pii/S1359836815002607

[30] M. Wisnom, Modelling discrete failures in composites with interface elements, Composites Part A: Applied Science and Manufacturing 41 (7) (2010) 795–805. doi:10.1016/j.compositesa.2010.02.011.
URL http://linkinghub.elsevier.com/retrieve/pii/S1359835X10000680

[31] S. Abrate, J. F. Ferrero, P. Navarro, Cohesive zone models and impact damage predictions for composite structures, Meccanica 50 (10) (2015) 2587–2620.

[32] F. Aymerich, F. Dore, P. Priolo, Prediction of impact-induced delamination in cross-ply composite laminates using cohesive interface elements, Composites Science and Technology 68 (12) (2008) 2383–2390. doi:10.1016/j.compscitech.2007.06.015.
URL http://linkinghub.elsevier.com/retrieve/pii/S0266353807002655

[33] D. Feng, F. Aymerich, Finite element modelling of damage induced by low-velocity impact on composite laminates, Composite Structures 108

(2014) 161–171. doi:10.1016/j.compstruct.2013.09.004.
URL http://linkinghub.elsevier.com/retrieve/pii/S0263822313004510

[34] S. Heimbs, S. Heller, P. Middendorf, F. Hhnel, J. Weie, Low velocity impact on CFRP plates with compressive preload: Test and modelling, International Journal of Impact Engineering 36 (10-11) (2009) 1182–1193. doi:10.1016/j.ijimpeng.2009.04.006.
URL http://linkinghub.elsevier.com/retrieve/pii/S0734743X09000797

[35] S. Heimbs, T. Bergmann, D. Schueler, N. Toso-Pentecte, High velocity impact on preloaded composite plates, Composite Structures 111 (2014) 158–168. doi:10.1016/j.compstruct.2013.12.031.
URL http://linkinghub.elsevier.com/retrieve/pii/S0263822313006612

[36] Y. Shi, C. Pinna, C. Soutis, Modelling impact damage in composite laminates: A simulation of intra- and inter-laminar cracking, Composite Structures 114 (2014) 10–19. doi:10.1016/j.compstruct.2014.03.052.
URL http://linkinghub.elsevier.com/retrieve/pii/S026382231400155X

[37] C. Bouvet, B. Castani, M. Bizeul, J.-J. Barrau, Low velocity impact modelling in laminate composite panels with discrete interface elements, International Journal of Solids and Structures 46 (1415) (2009) 2809–2821. doi:10.1016/j.ijsolstr.2009.03.010.
URL http://www.sciencedirect.com/science/article/pii/S002076830900136X

[38] P. Navarro, J. Aubry, S. Marguet, J.-F. Ferrero, S. Lemaire, P. Rauch, Semi-continuous approach for the modeling of thin woven composite panels applied to oblique impacts on helicopter blades, Composites

Part A: Applied Science and Manufacturing 43 (6) (2012) 871–879. doi:10.1016/j.compositesa.2012.01.020.
URL http://linkinghub.elsevier.com/retrieve/pii/S1359835X12000401

[39] P. Navarro, F. Pascal, J. Aubry, S. Marguet, J. F. Ferrero, S. Lemaire, P. Rauch, Semi-continuous approach for the study of impacts on woven composite laminates: Modeling interlaminar behavior with a specific interface element, International Journal of Impact Engineering 75 (2015) 184–193. doi:10.1016/j.ijimpeng.2014.08.012.
URL http://www.sciencedirect.com/science/article/pii/S0734743X14001912

[40] F. Pascal, P. Navarro, S. Marguet, J.-F. Ferrero, On the modelling of low to medium velocity impact onto woven composite materials with a 2d semi-continuous approach, Composite Structures 134 (2015) 302–310. doi:10.1016/j.compstruct.2015.08.067.
URL http://linkinghub.elsevier.com/retrieve/pii/S026382231500759X

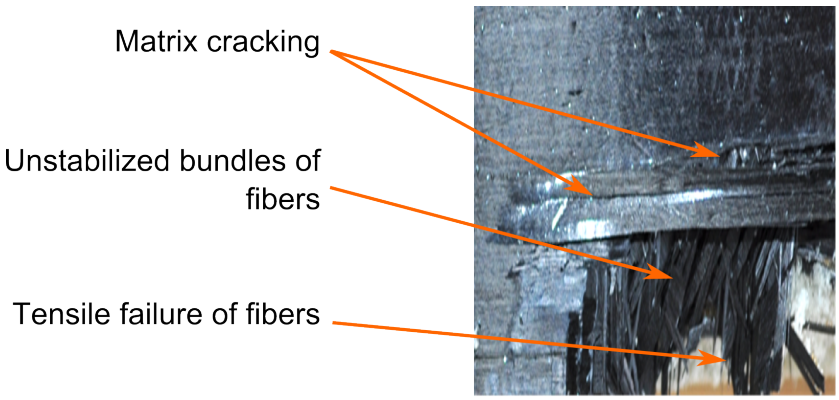

Figure 1: Fracture surface of a UD thin laminate after impact

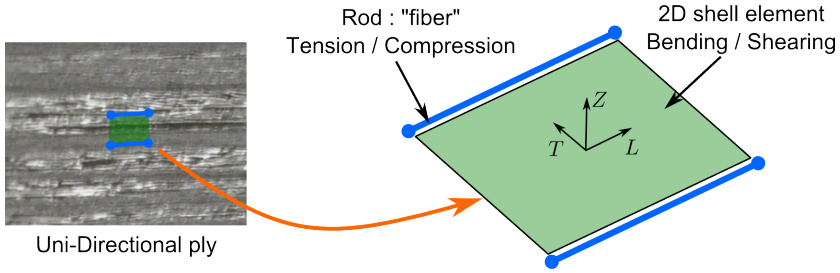

Figure 2: Semi-continuous strategy for the modelling of a UD ply

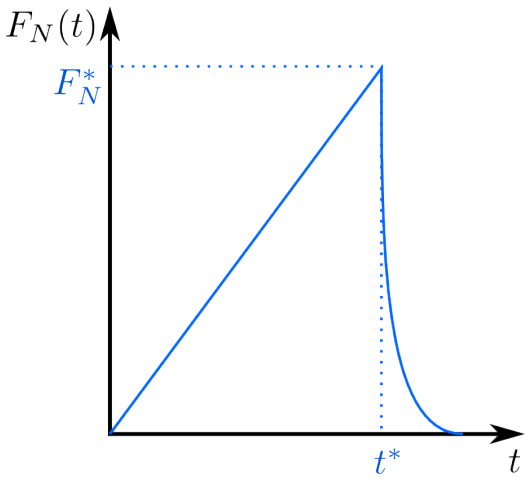

Figure 3: Brittle rupture of the rods with an exponential decreasing law

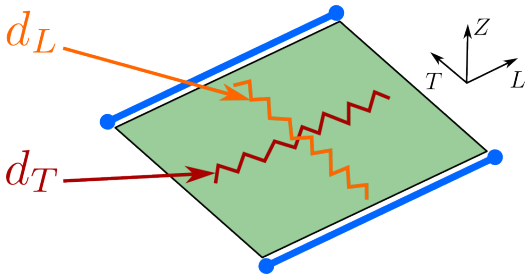

Figure 4: Longitudinal and transverse damage modelling

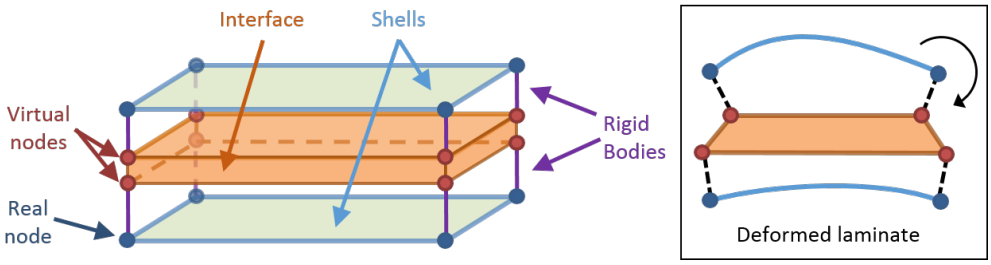

Figure 5: Principle of the specific shell-to-shell interface element used

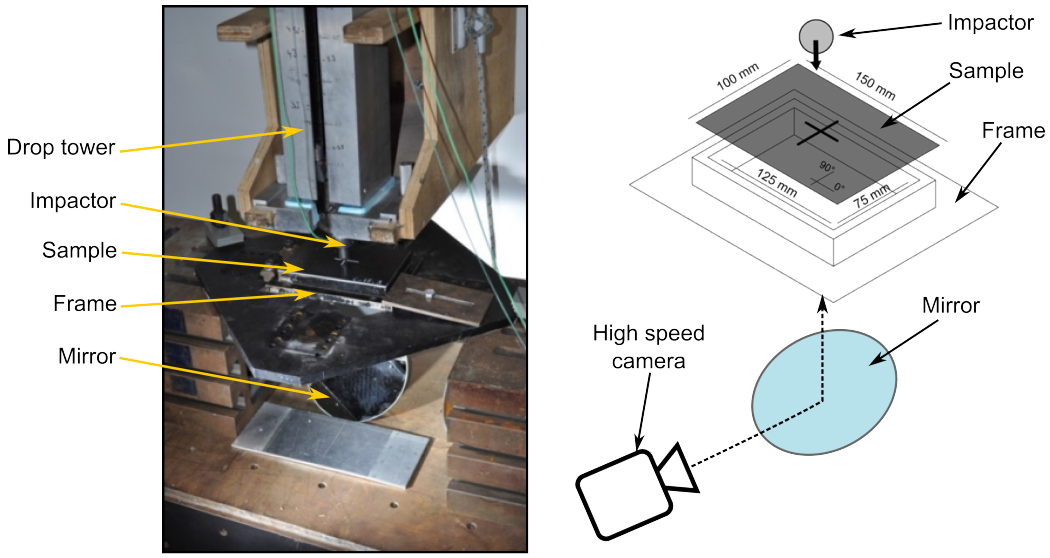

Figure 6: Drop weight device - Impact test description

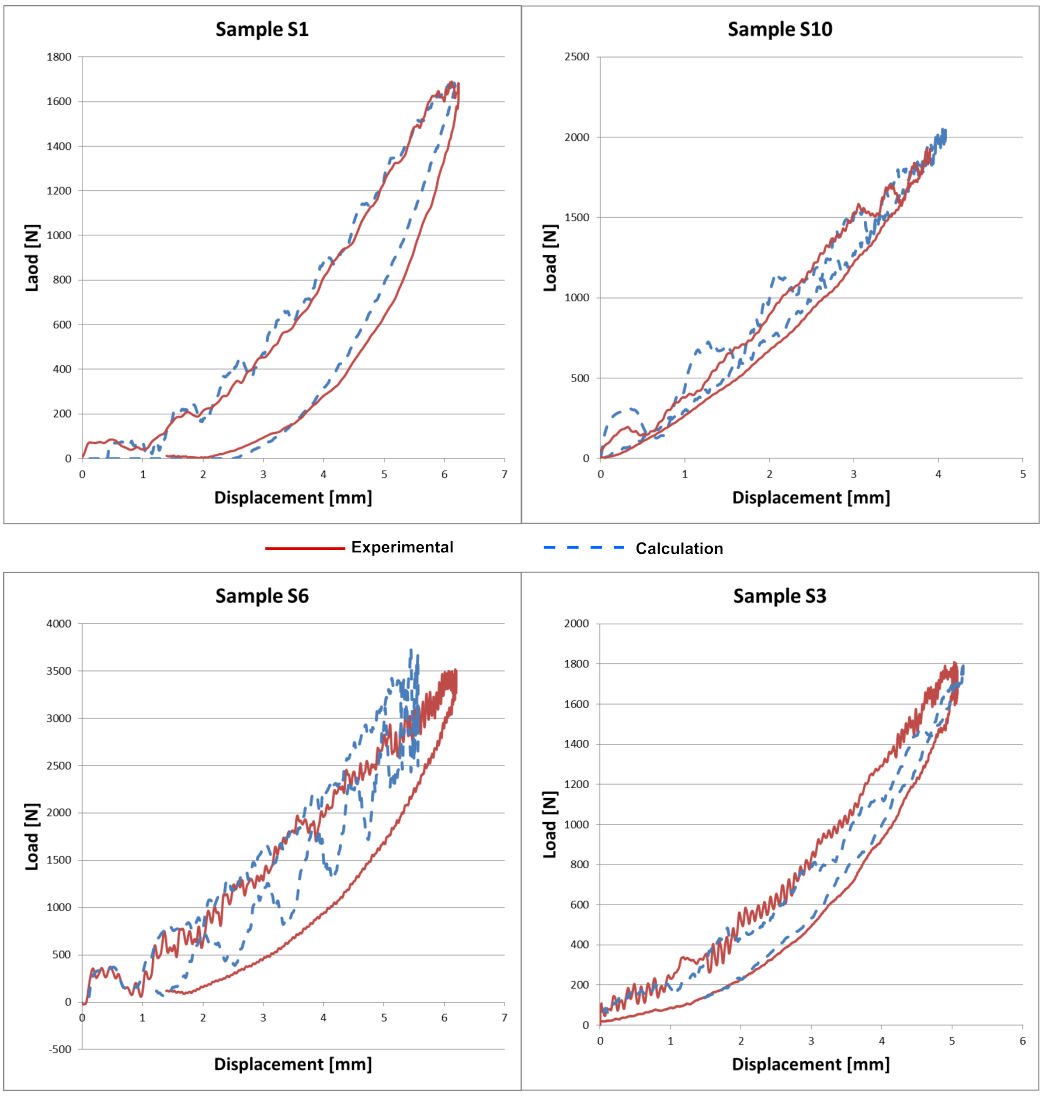

Figure 7: Load/Displacement curves for the samples S1, S3, S6 and S10.

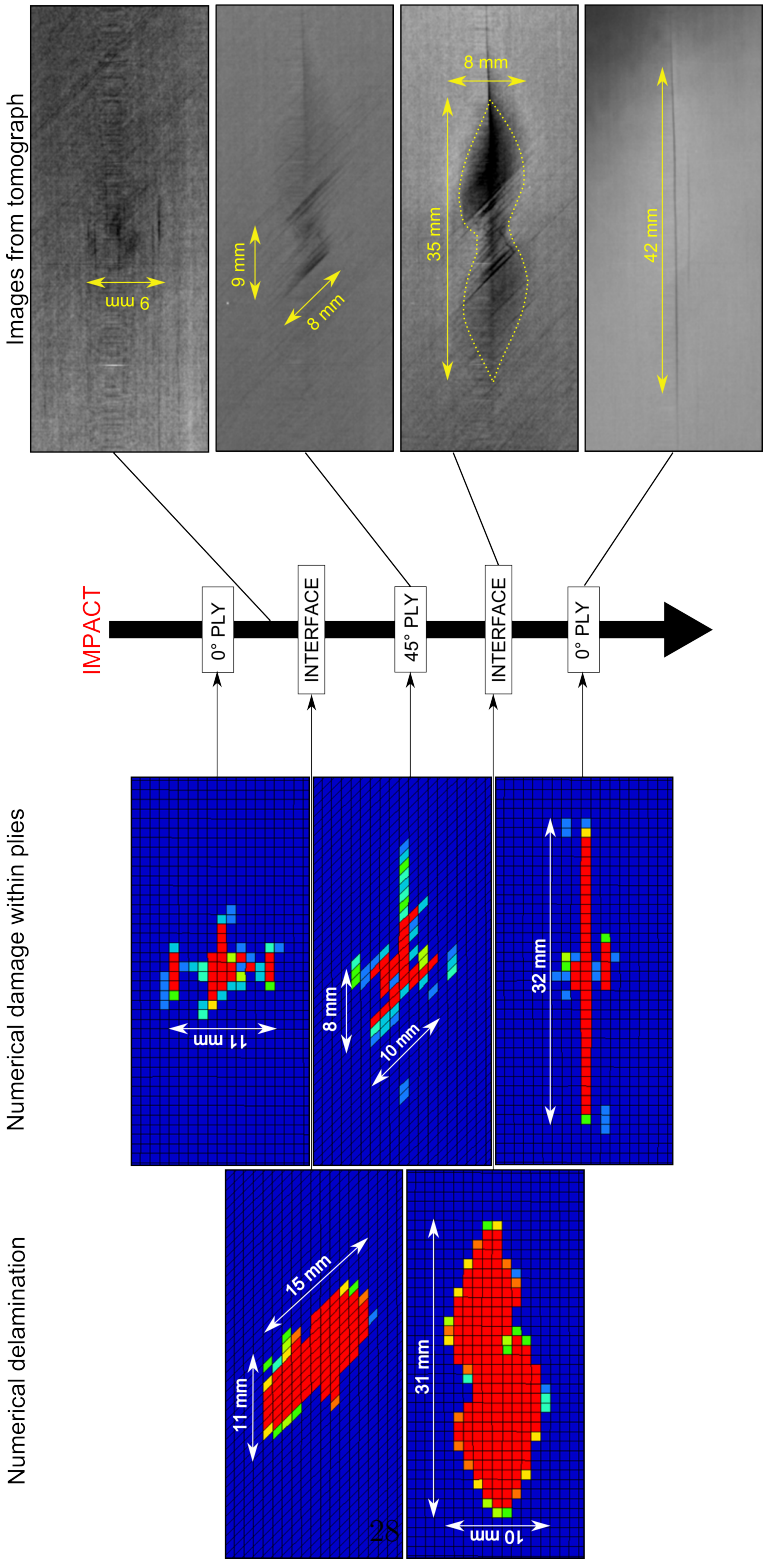

Figure 8: Experimental and numerical damages for configuration S3

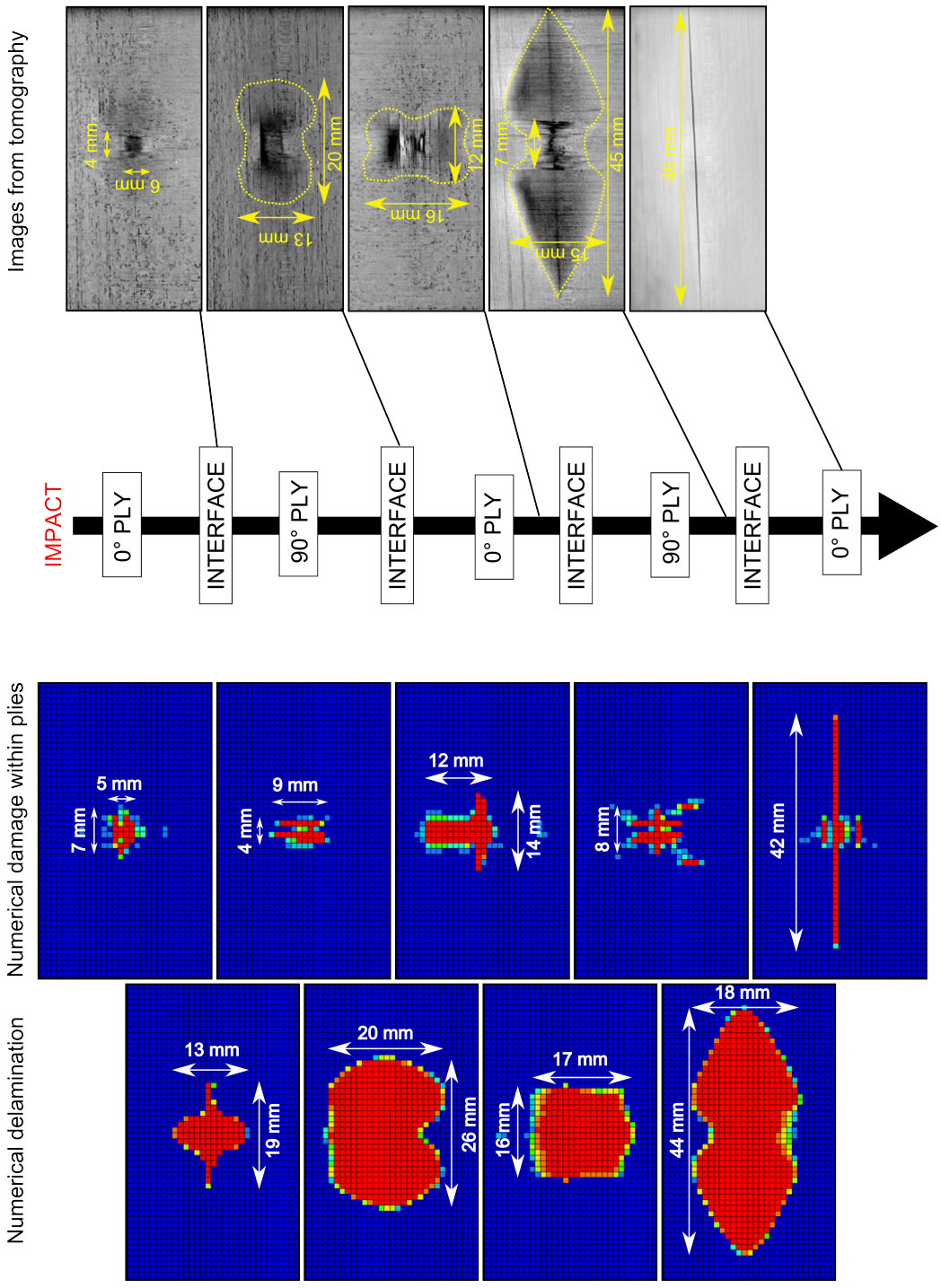

Figure 9: Experimental and numerical damages for configuration S6

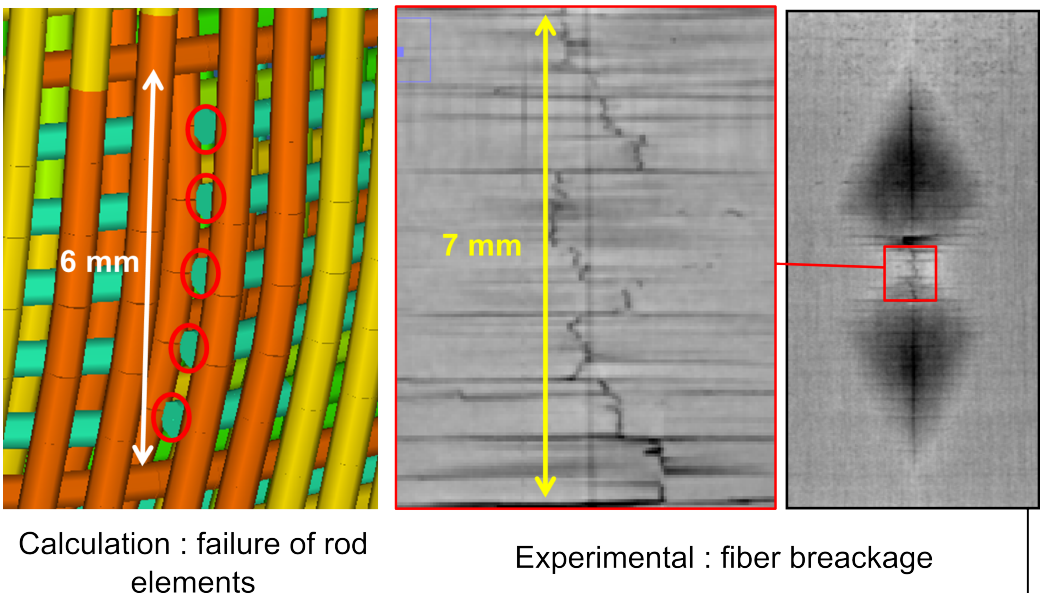

Figure 10: Fiber breackage for the specimen S8

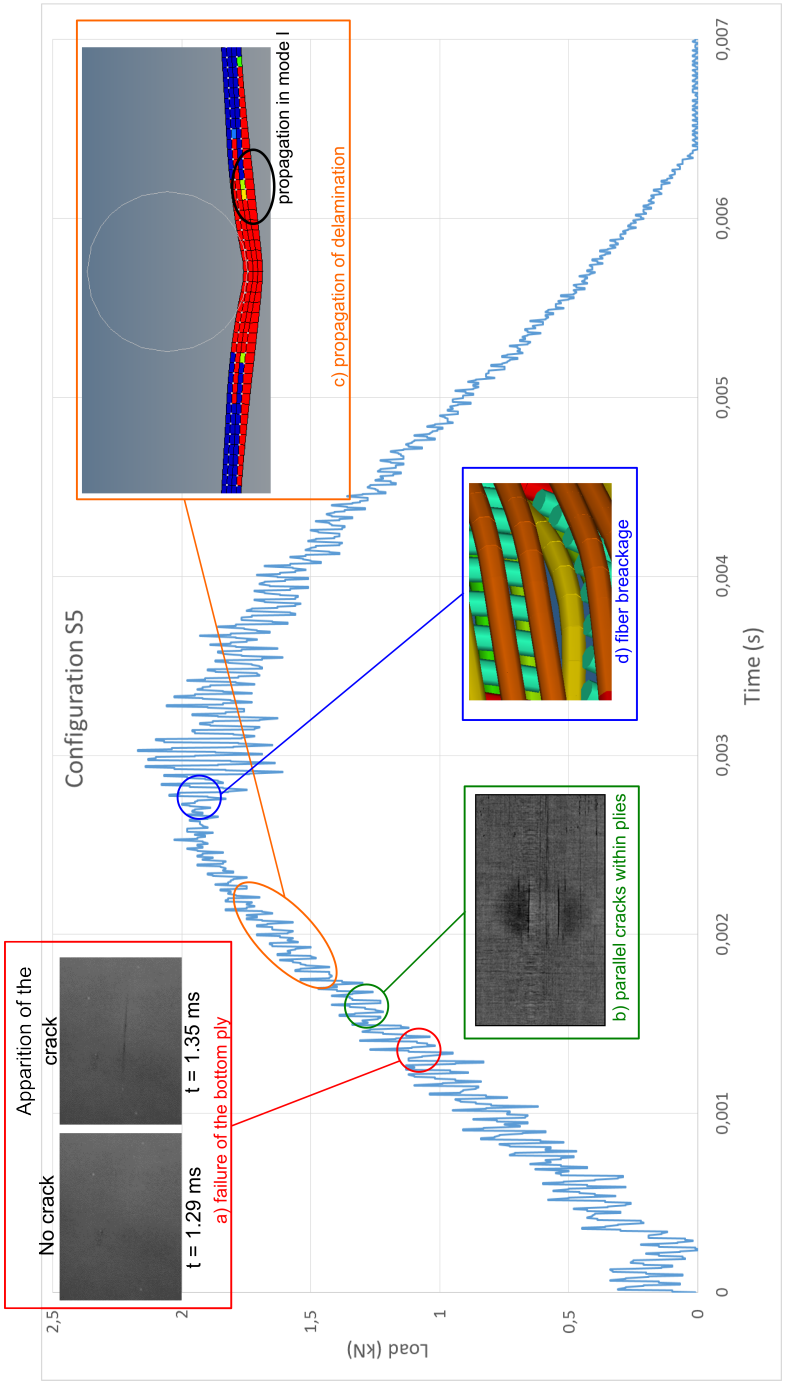

Figure 11: Damage mechanisms

Specimen	**Material**	**Stacking sequence**	**Thickness**	**Velocity**
S1	T700/M21	$[0_2, 90_2, 0_2]$	$1.44\,mm$	$2\,m.s^{-1}$
S2	T700/M21	$[90_2, 0_2, 90_2]$	$1.44\,mm$	$2\,m.s^{-1}$
S3	T700/M21	$[0_2, 45_2, 0_2]$	$1.44\,mm$	$2\,m.s^{-1}$
S4	T700/M21	$[90_2, 45_2, 90_2]$	$1.44\,mm$	$2\,m.s^{-1}$
S5	T700/M21	$[0_2, 90_2, 0_2, 90_2, 0_2]$	$2.4\,mm$	$2\,m.s^{-1}$
S6	T700/M21	$[0_2, 90_2, 0_2, 90_2, 0_2]$	$2.4\,mm$	$3\,m.s^{-1}$
S7	T700/M21	$[90_2, 0_2, 90_2, 0_2, 90_2]$	$2.4\,mm$	$2\,m.s^{-1}$
S8	T700/M21	$[90_2, 0_2, 90_2, 0_2, 90_2]$	$2.4\,mm$	$3\,m.s^{-1}$
S9	HTA7/913	$[0_2, 90_2, 0_2]$	$1.44\,mm$	$2\,m.s^{-1}$
S10	HTA7/913	$[0_2, 90_2, 0_2, 90_2, 0_2]$	$2.4\,mm$	$2\,m.s^{-1}$

Table 1: List of impacted configurations

Parameters for the ply modelling			
E_f	$255500\,MPa$	ε_{max}	$1.9\,\%$
V_f	0.57	Y_{OL}	$0.8\,J$
G_{LT}	$4500\,MPa$	Y_{CL}	$5\,J$
E_{Lm}	$1365\,MPa$	Y_{OT}	$0.5\,J$
E_{Tm}	$7260\,MPa$	Y_{CT}	$2\,J$
E_{Lb}	$147000\,MPa$	σ_0	$19\,MPa$
E_{Tb}	$7260\,MPa$	K_{plas}	$25\,MPa$
ν_{LT}	0.28	β	1
Parameters for the interface modelling			
σ_1	$60\,MPa$	G_{1C}	$0.32\,N.mm^{-1}$
σ_2	$60\,MPa$	G_{2C}	$1.1\,N.mm^{-1}$

Table 2: Parameters for the T700/M21 composite

Parameters for the ply modelling			
E_f	$220000\,MPa$	ε_{max}	$1.25\,\%$
V_f	0.59	Y_{OL}	$0.8\,J$
G_{LT}	$2000\,MPa$	Y_{CL}	$5\,J$
E_{Lm}	$1200\,MPa$	Y_{OT}	$0.5\,J$
E_{Tm}	$5860\,MPa$	Y_{CT}	$2\,J$
E_{Lb}	$131000\,MPa$	σ_0	$70\,MPa$
E_{Tb}	$5860\,MPa$	K_{plas}	$25\,MPa$
ν_{LT}	0.28	β	1
Parameters for the interface modelling			
σ_1	$40\,MPa$	G_{1C}	$0.28\,N.mm^{-1}$
σ_2	$40\,MPa$	G_{2C}	$1.6\,N.mm^{-1}$

Table 3: Parameters for the HTA7/913 composite

Specimen	$\mathbf{F_{max}}$	$\mathbf{u_{max}}$	$\mathbf{Ld_{max}}$
S1	0.2 %	0.9 %	16.2 %
S2	7.3 %	1.3 %	15.4 %
S3	1 %	1.6 %	11.4 %
S4	5.4 %	7.6 %	16.1 %
S5	1.7 %	2.3 %	8.3 %
S6	5.9 %	10.2 %	2.2 %
S7	2.8 %	0.3 %	12 %
S8	7.3 %	5.2 %	14.3 %
S9	6.8 %	1 %	13 %
S10	6.8 %	4.5 %	5.6 %

Table 4: Relative errors between experimental and numerical maximum load (F_{max}), maximum impactor displacement (u_{max}) and maximal size of delamination (Ld_{max})